

Document downloaded from:

<http://hdl.handle.net/10251/141286>

This paper must be cited as:

Giménez, JG.; Alonso Pazos, A.; Baeza González, LM. (2018). Precision analysis and dynamic stability in the numerical solution of the two-dimensional wheel/rail tangential contact problem. *Vehicle System Dynamics*. 57(12):1822-1846.  
<https://doi.org/10.1080/00423114.2018.1552365>



The final publication is available at

<https://doi.org/10.1080/00423114.2018.1552365>

Copyright Taylor & Francis

Additional Information

This is an Accepted Manuscript of an article published by Taylor & Francis in *Vehicle System Dynamics* on 2018, available online:  
<https://doi.org/10.1080/00423114.2018.1552365>

Precision analysis and dynamic stability in the  
numerical solution of the two-dimensional wheel/rail  
tangential contact problem

José Germán Giménez<sup>1</sup>, Asier Alonso<sup>1,2</sup>, Luis Baeza<sup>3\*</sup>

<sup>1</sup> TECNUN-Universidad de Navarra, Manuel Lardizábal 13, 20018 San Sebastián, Spain

<sup>2</sup> CAF i+D, S.A., J.M. Iturrioz 26, 20200 Beasain, Spain

<sup>3</sup> ISVR, University of Southampton, SO17 1BJ, UK

\* [L.Baeza@soton.ac.uk](mailto:L.Baeza@soton.ac.uk)

**Abstract**

In this paper the two-dimensional contact problem is analysed through different mesh topologies and strategies for approaching equations, namely; the collocation method, Galerkin, and the polynomial approach. The two-dimensional asymptotic problem (linear theory) associated with very small creepage (or infinite friction coefficient) is taken as a reference in order to analyse the numerical methods, and its solution is tackled in three different ways, namely; steady state problem, dynamic stability problem, and non-steady state problem in the frequency domain. In addition, two elastic displacements derivatives calculation methods are explored: analytic and finite differences.

The results of this work establish the calculation conditions that are necessary to guarantee dynamic stability and the absence of numerical singularities, as well as the parameters for using the method that allows for maximum precision at minimum computational cost to be reached.

**Keywords:**

Wheel/rail contact; rolling contact; precision analysis; variational theory; CONTACT.

## 1. INTRODUCTION

The study of the problem of two solids in rolling contact is common in different engineering areas (bearings, cranes, different types of vehicles, etc.) but railway dynamics is perhaps where its incidence has more importance. Simulation of railway vehicle dynamics, vehicle-track interaction and rolling noise [1], wear of wheels and rails [2], study of rolling contact fatigue, etc., are problems that cannot be analysed in depth without an accurate knowledge of displacements, local slip velocities and traction distributions that exist in wheel-rail contact.

The first important step in the investigation of the tangential rolling contact problem is, perhaps, the one due to Carter [3] who, in 1926, proposed an exact solution for the 2D contact traction problem of two infinite rolling cylinders with relative slip between them. After Carter's work, it is necessary to wait until 1964 when Kalker [4] developed a solution to the tangential rolling problem of two spherical solids. In his PhD thesis [5], Kalker himself gave a general solution to the steady state and asymptotic problem (linear theory) of rolling contact, which adopted the Hertz model as the normal contact solution. The linear theory is valid for infinitesimal creepages (or infinite friction coefficient). In Kalker's solution, the contact traction distribution is formulated by polynomial functions that are multiplied by the inverse of the normal traction field. This approach presents a singularity at the edge of the contact area that is necessary to adequately represent the tangential traction at the trailing edge of the contact area.

Also in Kalker's PhD thesis [5], using a similar approach for the traction distribution to those adopted in the asymptotic theory, the author solved the general contact problem for finite creepages and friction coefficient. The solution was only valid for elliptical contact areas and non-conformal contact conditions (Hertzian contact). In spite of this limitation, satisfactory solutions were obtained for different contact geometries and creepages; nevertheless the convergence of the solution was not always guaranteed.

In 1983 Kalker presented the variational theory [6, 7], which assumed non-Hertzian and non-conformal hypotheses. The variational theory is a simplified version of the boundary element method (BEM) in which the contact area is discretised by rectangular elements. In each element, the tractions are assumed to be constant and the derivatives in the kinematic relationships between local slip velocities and displacements in the contact are formulated through finite differences. In this model, the use of the collocation method, where the collocation points are at the interface between adjacent elements, avoids the need to impose boundary conditions in the formulation. The detailed explanation of this theory and its generalization to steady and non-steady state, linear and non-linear problems can be found in reference [8]. The convergence of the method is guaranteed in most cases if a constant friction coefficient is adopted [9]. The method still requires that the dimensions of the contact area are small in relation to the radii of curvature of the solids (non-conformal contact), and has, as its main drawback, its high computational cost.

In order to reduce the computational cost, different simplified theories have been developed. One of the best in terms of accuracy and computational cost is the Fastsim algorithm, which was published by Kalker in 1982 [10]. The literature shows different variants of this algorithm that have extended their use to cases with velocity-dependent friction coefficient and non-steady state contact problems [11, 12]; however the precision of such simplified theories in the calculation of the contact traction distribution and the local slip velocities is small [13]. Doubtless, the variational theory is the most precise approach for estimating relative displacements and contact traction distribution in rolling contact problems. The increasing computational power and the possibilities of parallel computing, make the implementation of the variational theory in dynamic simulation possible.

Although the first publication relating to the use of the variational theory dates from 1983 [5], to the authors' knowledge, a comparative analysis in terms of the accuracy and stability of this method remains unpublished. The optimal parameters and requirements with respect to the mesh topology, the points where the equations are satisfied (collocation points) and the boundary conditions implementation, have not been investigated in the literature associated with rolling contact mechanics. A study of this is fundamental to reduce the computational cost of the method whilst maintaining an acceptable level of precision. Nonetheless the literature shows works that develop discretisation error estimators in rolling contact finite element models that allow methodologies for  $h$ -refinement [14].

In this paper, different schemes are analysed in the application of the 2-dimensional BEM to rolling contact problems, evaluating which is the strategy that, for a required precision, needs less computational effort. It has also studied the conditions for which the resulting equations are dynamically stable. To carry out this study, the steady and the non-steady state asymptotic theories are used as reference solutions, which, due to the singularity of the stresses in the trailing edge of the contact area, can be considered the most critical from the point of view of precision in the calculation of the traction distribution. The obtained results serve as a guide for an efficient application of the BEM in advanced rolling contact problems for railway applications.

The structure of this work is described next. Section 2 presents the formulation of contact kinematics and the constitutive equations that allow modelling 2D rolling contact through BEM. Section 3 presents four contact problem resolution procedures, two of which are unpublished, namely; the collocation method due to Kalker, the Galerkin formulation applied to the rolling contact problem, the Knothe and Groß-Thebing method (which is the collocation method when a harmonic creepage is considered), and an approach for the non-steady state case based on the polynomial formulation of the traction and the displacement fields. Section 4 details the most important methodologies that will be studied throughout Sections 5 (for the stationary) and 6 (non-steady state case). The most relevant conclusions of this work are discussed in Section 7.

## 2. ROLLING CONTACT EQUATIONS FOR THE 2D CASE

In order to model the rolling contact problem of an infinite elastic cylinder on a half space, an inertial frame of reference  $\mathbf{xyz}$  is defined, where its origin is the centre of the contact area, axis  $\mathbf{x}$  has the rolling (or longitudinal) direction and axis  $\mathbf{z}$  is normal to the contact plane, positive upward. The kinematic (or slip) equation at the contact area for the longitudinal  $\mathbf{x}$  direction is [8]:

$$s = \xi V - V \frac{\partial u}{\partial x} + \frac{\partial u}{\partial t}, \quad (1)$$

$s$  being the local slip velocity in the  $\mathbf{x}$  direction,  $u$  the relative longitudinal displacements between rail and wheel from the undeformed to the deformed configurations,  $\xi$  the longitudinal creepage and  $V$  the wheel speed (neither lateral creepage nor spin are considered in the present study). The asymptotic theory assumes that the friction coefficient is infinite and consequently the local slip velocity is null. In such a case, the kinematic equations can be rewritten as follows:

$$0 = \xi - \frac{\partial u}{\partial x} + \frac{1}{V} \frac{\partial u}{\partial t}. \quad (2)$$

In order to obtain the constitutive equations, the Cerruti relationship is chosen as the fundamental solution that formulates the displacements of one elastic halfspace due to punctual loads:

$$U(x, y) = \frac{1}{\pi G (x^2 + y^2)^{3/2}} (x^2 + (1-\nu)y^2) F, \quad (3)$$

where  $G$  and  $\nu$  are respectively the shear modulus and the Poisson ratio of the solids material,  $(x, y)$  are the coordinates where the longitudinal displacement  $U$  is measured, and  $F$  is the total longitudinal force that is transmitted between the solids at the origin  $(x, y) = (0, 0)$ . The last equation can be compacted as follows:

$$U(x, y) = K(x, y) F. \quad (4)$$

In the 2D problem, the displacement and the traction distributions do not depend on the lateral co-ordinate  $y$ . The displacements associated with the elastic deformation  $u(x)$  are assumed to be due to the contact traction distribution,  $p(x)$  that is applied in the contact area. Consequently, the following constitutive equation is found:

$$u(x) = \iint_S K(x - \alpha, -\beta) p(\alpha) d\alpha d\beta, \quad (5)$$

$S$  being the contact area domain (depending on the integral domain and the traction distribution, the integral in the last equation may not converge).

The convective term  $\partial u / \partial x$  is deduced from the last equation as follows:

$$\frac{\partial u(x)}{\partial x} = \iint_s K'(x - \alpha, -\beta) p(\alpha) d\alpha d\beta, \quad (6)$$

where:

$$K'(x, y) = \frac{-x^3 - (1 - 3\nu)x y^2}{\pi G (x^2 + y^2)^{5/2}}. \quad (7)$$

From these formulae, Eq. (2) can be expressed through the following matrix form:

$$\iint_s K'(x - \alpha, -\beta) p(\alpha) d\alpha d\beta - \frac{1}{v} \iint_s K(x - \alpha, -\beta) \frac{dp(\alpha)}{dt} d\alpha d\beta = -\xi. \quad (8)$$

### 3. SOLUTION OF THE TANGENTIAL CONTACT PROBLEM

Equation (8) must be satisfied at any point of the contact area. This is an integral equation in which the unknown is the longitudinal traction distribution  $p(x, t)$  that acts in the interface between the solids in contact. The present work adopts a rectangular contact area,  $2a \times 2b$ , where the lateral dimension  $2b$  is much bigger than the corresponding longitudinal one (which is an approximation of the 2D case).

The present Section presents four different techniques for calculating the tangential traction distribution: (1) the simplified version of the BEM proposed by Kalker in [5], which is used as basis for implementing (2) the Galerkin method; (3) the formulation proposed by Knothe and Groß Thebing [15] (actually the collocation method when the creepage is harmonic), which is used for presenting (4) a polynomial approach for calculating the contact traction distribution when the creepage varies harmonically.

The version of the BEM proposed in [7] discretises the contact area in elements, as can be seen in Fig. 1. The longitudinal coordinate of the  $e$ -th element centre is  $x_e$ , and its dimension  $\Delta x_e$  as shown in the figure. The tangential traction distribution is supposed to be constant into each element of the mesh. The tangential traction can be approached as follows:

$$p(x, t) = \sum_{e=1}^n N_e(x) p_e(t), \quad (9)$$

where  $n$  is the number of elements,  $p_e(t)$  is the constant tangential traction in the  $e$ -th element, and  $N_e$  is the form function associated with the  $e$ -th element; more explicitly, this function is:

$$N_e(x) = \begin{cases} 1 & \text{if } x_e - \Delta x_e / 2 < x \leq x_e + \Delta x_e / 2 \\ 0 & \text{otherwise} \end{cases}. \quad (10)$$

By substituting Eq. (9) into (8), one gets:

$$\sum_{e=1}^n \left\{ \iint_{S_e} K'(x-\alpha, -\beta) N_e(\alpha) d\alpha d\beta p_e - \frac{1}{v} \iint_{S_e} K(x-\alpha, -\beta) N_e(\alpha) d\alpha d\beta \dot{p}_e \right\} = -\xi, \quad (11)$$

$S_e$  being the contact area of the  $e$ -th element.

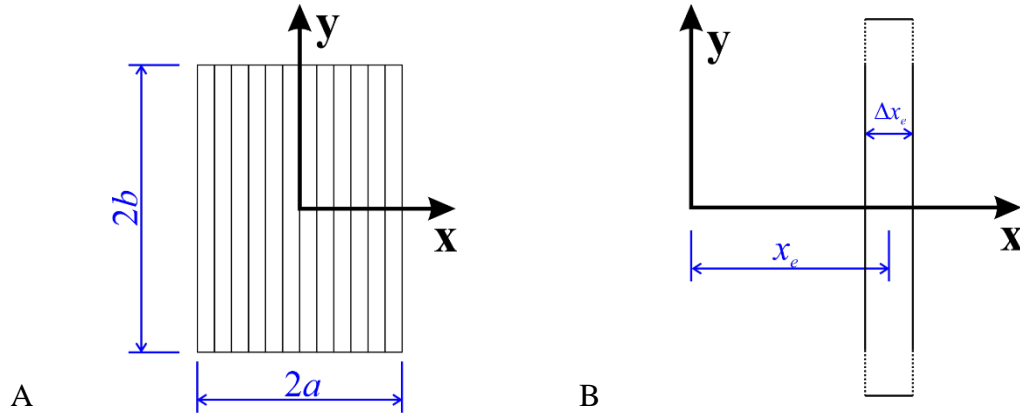


Fig. 1: Sketch of the BE mesh. A) Mesh and frame of reference. B) Zommed view of the  $e$ -th element.

Considering that the unknowns are  $p_e$ , for  $e = 1, \dots, n$ , following a collocation method, it is proceeded to impose Eq. (11) at  $n$  points of the contact area. Following this technique, the integral equation can be transformed in an ordinary differential equation system:

$$\mathbf{G}' \mathbf{p} - \frac{1}{v} \mathbf{G} \dot{\mathbf{p}} = -\xi, \quad (12)$$

where  $\mathbf{p}$  contains the tractions in  $n$  points of the mesh. Matrix  $\mathbf{G}$  is obtained from the first integral in Eq. (11) as follows:

$$G_{\ell m} = \int_{-b}^b \int_{x_m - \Delta x_m / 2}^{x_m + \Delta x_m / 2} K(\bar{x}_\ell - \alpha, -\beta) N_m(\alpha) d\alpha d\beta. \quad (13)$$

Vector  $\xi$  contains the longitudinal creepage in all its components, and  $\bar{x}_\ell$  is the coordinate of the  $\ell$ -th collocation point. Matrix  $\mathbf{G}'$  is computed in a similar way to Eq. (13), by changing  $K$  to  $K'$ .

The derivatives and integrals in Eq. (12) can be obtained analytically. However Kalker proposed to obtain the derivatives in  $\mathbf{K}'$  by finite differences.

Matrices  $\mathbf{G}'$  and  $\mathbf{G}$  are also computed in the present work by application of the Galerkin method by using  $N_e$  as test functions. For example, the expression for  $\mathbf{G}$  is:

$$G_{\ell m} = \frac{1}{\Delta x_\ell} \int_{x_\ell - \Delta x_\ell / 2}^{x_\ell + \Delta x_\ell / 2} \int_{-b}^b \int_{x_m - \Delta x_m / 2}^{x_m + \Delta x_m / 2} K(\bar{x}_\ell - \alpha, -\beta) N_m(\alpha) N_\ell(\delta) d\alpha d\beta d\delta \quad (14)$$

The calculation of  $\mathbf{G}'$  and  $\mathbf{G}$  through the Galerkin method is computed numerically through Gaussian quadrature. It must be pointed out that Galerkin and the original collocation method proposed by Kalker produces the same result if one single Gauss point is adopted in the quadrature.

From Eq. (12), the solution for the steady state case is obtained from the following equation:

$$\mathbf{p} = -(\mathbf{G}')^{-1} \boldsymbol{\xi}. \quad (15)$$

The complex response for the harmonic creepage variation is:

$$\mathbf{p}(\omega) = -\left(\mathbf{G}' - \frac{i\omega}{V} \mathbf{G}\right)^{-1} \boldsymbol{\xi}(\omega). \quad (16)$$

For steady state conditions, Kalker [5] solved this equation for elliptical contact areas by approaching the displacements  $\mathbf{u}$  by means of polynomial functions. According to the generalisation of Galin's theorem [16], the tangential traction field is formulated through polynomial functions multiplied by the inverse of the normal tractions. The calculation of the polynomial coefficients is carried out by imposing the constitutive relationships and minimizing the value of the tangential traction at the leading edge of the contact ellipse. This technique can be adopted for calculating the response to a harmonic creepage, as is presented here. Following this methodology, the tangential traction distribution can be approached through the next polynomial function:

$$p(x) = \sum_{j=0}^m c_j P_j(x), \quad (17)$$

where  $c_j$  denotes constants, and:

$$P_j(x) = \frac{1}{\sqrt{1 - \left(\frac{x}{a}\right)^2}} \left(\frac{x}{a}\right)^j. \quad (18)$$

From Galin's theorem, the displacement  $U_j(x)$  due to the  $j$ -th polynomial term  $P_j(x)$  has an exact solution which is a degree-  $j$  polynomial, and that is:

$$U_j(x) = \sum_{\ell=0}^j B_{j\ell} \left(\frac{x}{a}\right)^\ell, \quad (19)$$

$B_{j\ell}$  being constants, which form a matrix  $\mathbf{B}$  that is lower triangular.

The displacement  $U_j(x)$  can also be calculated from the Boussinesq-Cerrutti integral, which for the 2D problem is:

$$U_j(x) = \frac{1}{\pi G} \int_{-a}^a P_j(\alpha) \left( (1-\nu) \log \frac{4b^2}{(x-\alpha)^2} + 2\nu \right) d\alpha. \quad (20)$$

$B_{j\ell}$  is then calculated numerically, by making equal Eqs. (19) and (20) in a set of points of the contact area, and solving by least squares.

The displacements due to the tangential traction distribution Eq. (17) is:

$$u(x) = \sum_{j=0}^m c_j U_j(x), \quad (21)$$

and, from Eq. (19):

$$u(x) = \sum_{\ell=0}^m \left\{ \left( \frac{x}{a} \right)^\ell \sum_{j=0}^m c_j B_{j\ell} \right\}. \quad (22)$$

The last result can be adopted in the kinematic equation Eq. (2) for a harmonic creepage, which is:

$$0 = \xi(\omega) - \frac{\partial u}{\partial x} + \frac{i\omega}{V} u, \quad (23)$$

obtaining:

$$0 = \xi - \sum_{\ell=1}^m \left\{ \left( \frac{x}{a} \right)^{\ell-1} \frac{1}{a} \sum_{j=0}^m c_j B_{j\ell} \right\} + \frac{i\omega}{V} \sum_{\ell=0}^m \left\{ \left( \frac{x}{a} \right)^\ell \sum_{j=0}^m c_j B_{j\ell} \right\}. \quad (24)$$

Eq. (24) will be satisfied for each polynomial term, providing for the zero order polynomial term:

$$0 = \xi - \frac{1}{a} \sum_{j=0}^m c_j B_{j1} + \frac{i\omega}{V} \sum_{j=0}^m c_j B_{j0}, \quad (25)$$

and, for the  $\ell$ -th polynomial term ( $\ell > 0$ ):

$$0 = -\frac{1}{a} \sum_{j=0}^m c_j B_{j,\ell+1} + \frac{i\omega}{V} \sum_{j=0}^m c_j B_{j\ell}. \quad (26)$$

In order to satisfy that the traction is null at the leading edge of the contact area,  $p(a) = 0$  from Eqs. (17) and (18), the following equation must be fulfilled:

$$0 = \sum_{j=0}^m c_j. \quad (27)$$

The solution of the algebraic equation system formed by Eqs. (25), (26) and (27) provides the coefficients  $c_j$  and, subsequently, the longitudinal traction distribution  $p(x)$ .

#### 4. STRATEGIES FOR ASSESSING THE PRECISION OF THE METHODS

The resolution of Eqs. (15) and (16) has been carried out in this paper by following different strategies; these are:

- i. Collocation method where the collocation points are in the centre of the elements. In addition, the boundary conditions are applied, which are null traction in the elements at the leading edge of the contact area, and sliding conditions in the cells at the trailing edge. It is the strategy used by Knothe and Groß-Thebing in Ref. [15].
- ii. Collocation method where the collocation points are in the leading border of each element. It is the procedure adopted by Kalker in his variational theory [7]. No boundary condition is imposed.
- iii. Collocation method where the collocation points are in coordinate  $x_e + \Delta x_e \alpha$ ,  $\alpha$  being a parameter that adopts values in the range  $]0,1[$ . In this strategy, no boundary conditions are imposed. NB: this is a generalisation of strategy ii.
- iv. Galerkin method through which the error is minimised in the whole domain, weighted by the form functions Eq. (10). Also in this case, different cases associated with the quadrature points will be analysed.

Fig. 2 shows one longitudinal strip of the mesh where variable  $\alpha$  has different values for the leading  $\alpha_L$  and trailing  $\alpha_T$ . Instead of a constant  $\alpha$  value for the inner elements,  $\alpha$  is calculated following a linear interpolation between the leading and trailing values, thus:

$$\alpha = \alpha_L \frac{x_e - x_T}{x_L - x_T} + \alpha_T \frac{x_L - x_e}{x_L - x_T}, \quad (28)$$

$x_L$ ,  $x_T$  and  $x_e$  being the  $\mathbf{x}$ -coordinates of the leading element centre, the trailing element centre and the current element centre, respectively. When the Galerkin method is implemented, the coordinates  $x_e + \Delta x_e \alpha$  are set as the central point for Gauss quadrature.

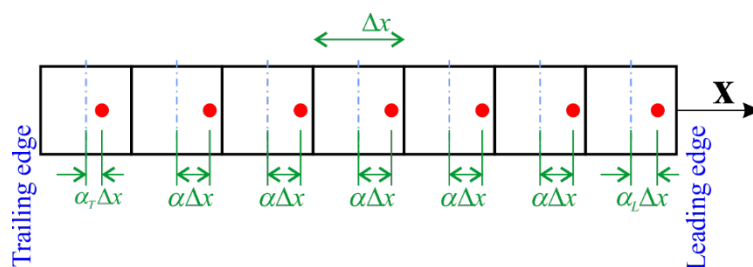


Fig. 2: Collocation points (red dots) in the mesh.

The calculation of the derivative of the elastic displacements with respect to  $x$ -coordinate  $\partial u / \partial x$  has been calculated in two different ways, namely:

- I. Analytical calculation of the derivative.
- II. Finite differences, by means of the expression

$$\left. \frac{\partial u}{\partial x} \right|_{x=x_e} = \frac{u(x_e + \Delta x_e) - u(x_e)}{\Delta x_e}. \quad (29)$$

With regard to the use of option I, the elements present a singularity in the calculation of the value  $\partial u / \partial x$  in the edge of the elements. This singularity is represented in Fig. 3 in which the derivative of the displacement tends to infinity at the element border  $x = x_e + \Delta x_e / 2$ . The presence of this singularity makes it difficult to use strategies based on the analytical calculation of the derivatives and favours the use of finite-differences.

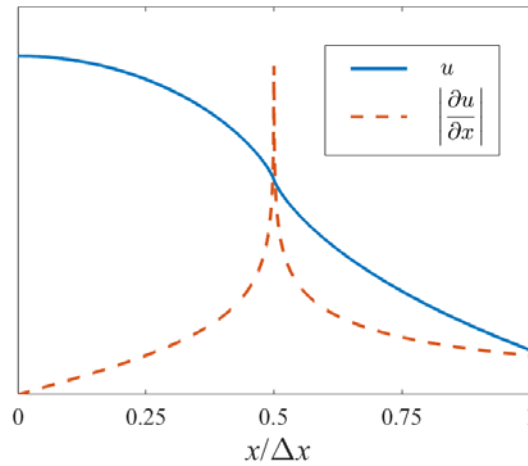


*Fig. 3: Displacement field and its derivative in an elastic half space due to a constant traction distribution on a rectangular element. The derivative presents a singularity in the element edge  $x = \Delta x / 2$ .*

Another key aspect that will be analysed in the following sections is the mesh topology. The following topologies have been considered:

- A. Mesh with equal size rectangular elements (see Fig. 4.A).
- B. Mesh with variable sizes in geometric growth (Fig. 4.B).
- C. Mesh adopted by Knothe and Groß-Thebing that reduces the size of the elements located at the ends of each strip (Fig. 4.C).
- D. The Knothe and Groß-Thebing case but only reducing the size of the cell in the trailing edge (Fig. 4.D). This topology will be referred to in the present paper as ‘*modified Knothe*’.

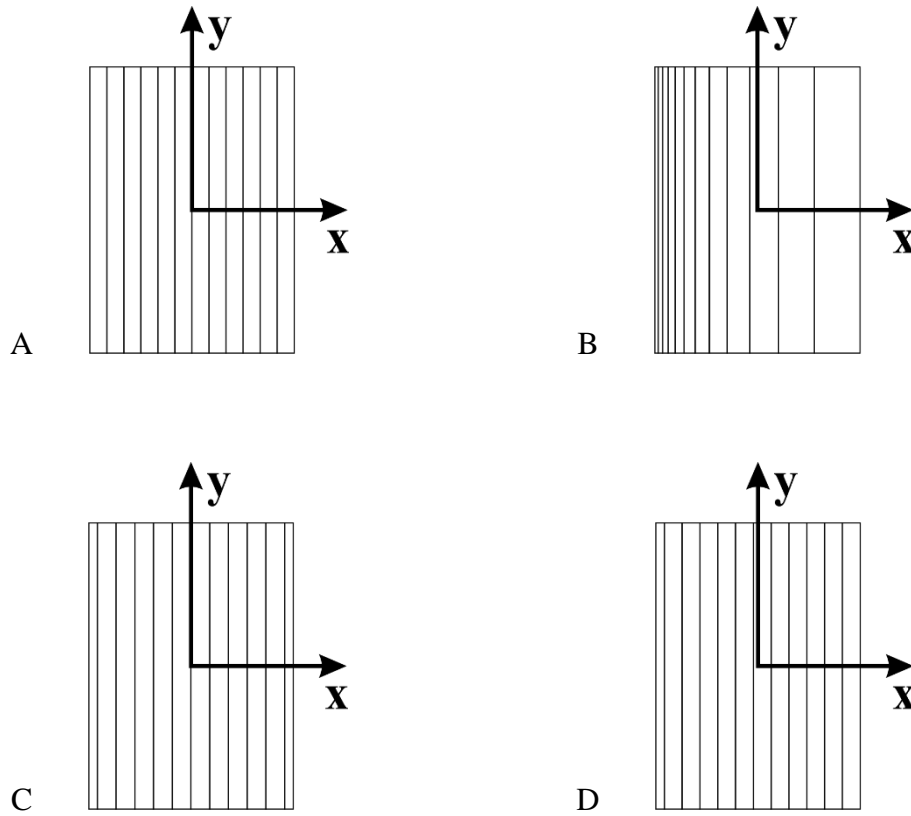


Fig. 4: Different mesh topologies for the contact area. A) Mesh with constant-size elements. B) Geometric refinement. C) Knothe and Groß-Thebing's mesh, where the leading and trailing elements are smaller. D) Modified Knothe topology, where the trailing elements are smaller.

The following sections will analyse the above-mentioned strategies in order to assess the precision in the calculation of the contact traction distribution, the steady and unsteady creep coefficients, and the dynamic stability.

## 5. STUDY FOR THE 2D STEADY STATE CASE

This section investigates a steady state 2D rolling contact, through an approach that considers a finite rectangular area,  $2a \times 2b$ , being the rolling dimension  $2a$  much smaller than the lateral direction  $2b$ . By adopting the asymptotic hypotheses, the traction force density in the rolling direction  $\bar{F}_x$  (total force divided by the lateral dimension length  $2b$ ) is related to the longitudinal creepage  $\xi_x$  by means of the following formula:

$$\bar{F}_x = -a G c_{11} \xi_x, \quad (30)$$

$G$  being the combined shear modulus of the wheel/rail materials, and  $c_{11}$  the longitudinal creep coefficient (also known as Kalker's coefficient). The creep coefficient has a closed form solution for the 2D problem (see Ref. [5]), which is:

$$c_{11} = \frac{\pi^2}{4(1-\nu)}. \quad (31)$$

In the following figures, the creep coefficient obtained numerically  $c_{11}^*$  through different approaches that were described in section 4, is compared with the exact solution  $c_{11}$  from Eq. (31).

### 5.1. Collocation method

Fig. 5 presents  $c_{11}^*/c_{11}$  ratio vs. parameter  $\alpha$ , where the equations have been solved through the collocation method, using the finite difference formula for obtaining the derivatives  $\partial u / \partial x$ . In these studies, the parameters  $\alpha$  for the leading ( $\alpha_L$ ) and trailing ( $\alpha_T$ ) elements are fixed whereas  $\alpha$  is computed for the inner elements through Eq. (23).

Fig. 5.A has been carried out for one mesh with  $n=40$  elements and analyses the influence of  $\alpha$  following three schemes:

- $\alpha = \alpha_L = \alpha_T$ .
- $\alpha = \alpha_T$  and  $\alpha_L = 0$ .
- $\alpha = \alpha_L$  and  $\alpha_T = 0$ .

It can be seen that curve  $\alpha = \alpha_L = \alpha_T$  presents its maximal accuracy for  $\alpha=0.5$ . In precise terms, Kalker adopted  $\alpha = 0.5$  when he implemented the variational theory in CONTACT algorithm. The curve where  $\alpha_T = 0$  is the less accurate strategy, whereas the curve  $\alpha_L = 0$  is the more precise and presents an optimal result when  $\alpha_T = 0.63$ . The influence of the number of elements in the mesh for  $\alpha_L = 0$  is analysed in Fig. 5.B, where  $c_{11}^*/c_{11}$  ratio vs  $\alpha$  is represented. It can be seen that  $\alpha = \alpha_T = 0.63$  and  $\alpha_L = 0$  is an optimal for the 2D case, independently of the number of elements that are studied.

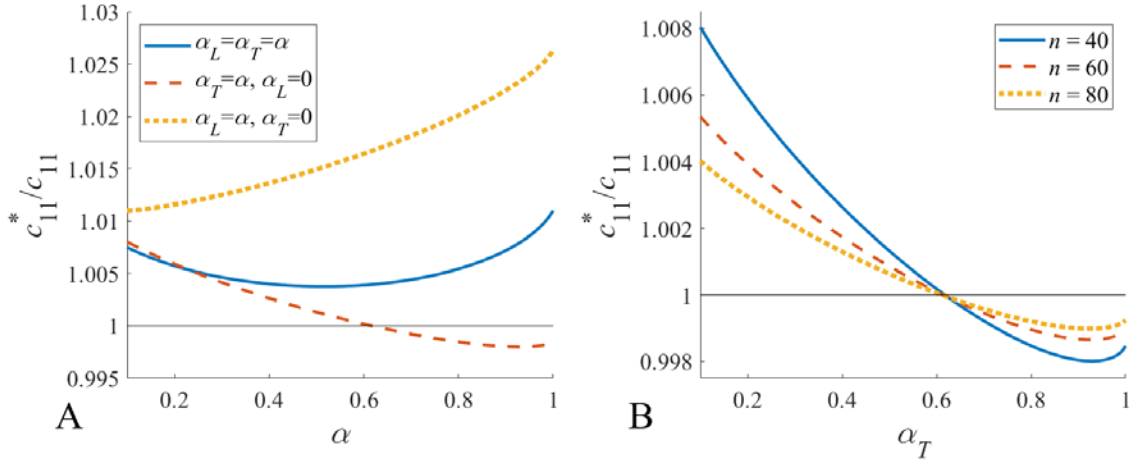


Fig. 5:  $c_{11}^*/c_{11}$  ratio as a function of the collocation parameter  $\alpha$ . The derivative  $\partial u / \partial x$  is calculated through finite differences. A) Collocation method by means of three approaches:  $\alpha_L = \alpha_T = \alpha$ ;  $\alpha_L = \alpha$  and  $\alpha_T = 0$ ;  $\alpha_T = \alpha$  and  $\alpha_L = 0$ . The number of elements is  $n = 40$ . B) Collocation method by adopting  $\alpha_L = \alpha$  and  $\alpha_T = 0$ , for three different number of elements:  $n = 40$ ,  $n = 60$  and  $n = 80$ .

Fig. 6 presents a study of the mesh refinement and its influence on the precision of the collocation method. The plots represent  $c_{11}^*/c_{11}$  ratio versus the number of elements  $n$  in the mesh. Fig. 6.A corresponds with studies where the derivatives  $\partial u / \partial x$  have been approached by means of finite differences. Three  $\alpha_L$  and  $\alpha_T$  combinations that are initially considered favourable have been studied. Parameter  $\alpha$  for the inner elements is interpolated from  $\alpha_L$  and  $\alpha_T$  through Eq. (28). It can be seen that all the cases converge to the exact solution; however the rate of convergence is bigger for  $\alpha_L = 0$  and  $\alpha_T = 0.63$ , much better than  $\alpha = \alpha_L = \alpha_T = 0.5$  used in the original CONTACT method. Errors smaller than 0.01% are obtained for  $n = 20$  elements. Fig. 6.B includes results corresponding to the exact calculation of the derivatives and three combinations of  $\alpha_L$ ,  $\alpha$  and  $\alpha_T$ , that avoids the singularity when  $\alpha = 0.5$  (discussed in Fig. 3). These results are less precise than the ones presented in Fig. 6.A.

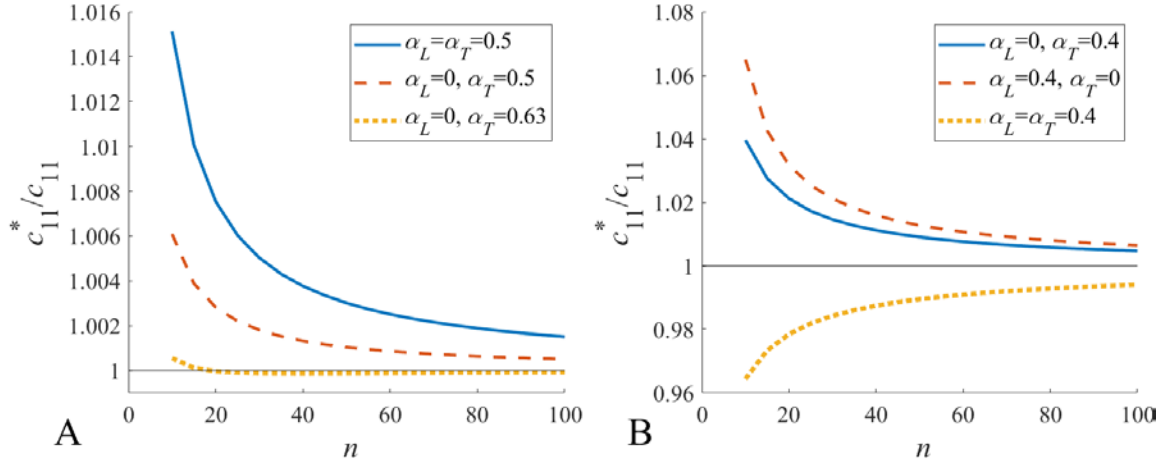


Fig. 6:  $c_{11}^*/c_{11}$  ratio as a function of the number of elements in the mesh  $n$ , by following the collocation method. A) The derivatives  $\partial u / \partial x$  are calculated by means of finite differences, and three combinations of collocation parameter:  $\alpha_L = \alpha_T = 0.5$ ;  $\alpha_L = 0$  and  $\alpha_T = 0.5$ ;  $\alpha_L = 0$  and  $\alpha_T = 0.63$ . B) The derivatives  $\partial u / \partial x$  are calculated analytically, and three combinations of collocation parameter:  $\alpha_L = 0$  and  $\alpha_T = 0.4$ ;  $\alpha_L = 0.4$  and  $\alpha_T = 0$ ; and  $\alpha_L = \alpha_T = 0.4$ .

Fig. 7 is analogous to Fig. 5, but the analytical form of the derivative  $\partial u / \partial x$  is used instead of the finite differences formula. In order to avoid the singularity when the closed form of the derivative is adopted, the derivative in the interval  $0.499 < \alpha \leq 0.5$  will be assumed to be the derivative at  $\alpha = 0.499$ , whereas the value in  $0.5 < \alpha < 0.501$  will be the derivative at  $\alpha = 0.501$ . It can be seen in Fig. 7.A that for the curve  $\alpha_L = \alpha_T = 0.5$  there is a minimum of precision at  $\alpha = 0.5$  caused by the influence of the singularity in the calculation of the derivative  $\partial u / \partial x$  at the element edge (as shown in Fig. 3). On the contrary, for curves where  $\alpha_L$  or  $\alpha_T$  is zero, the results are more accurate in the range  $\alpha \in [0.4, 0.6]$ . When  $\alpha > 0.7$  the results are more accurate for the curve corresponding to  $\alpha_L = 0$ .

For the curve  $\alpha_L = 0$ , the numerical coefficient  $c_{11}^*$  fits the theoretical one  $c_{11}$  in two points. This behaviour can be seen in Fig. 7.B, where the curve for  $\alpha_L = 0$  is plotted for three mesh densities ( $n = 40, 60$  and  $80$  elements). It can be seen that the point at which it has reached the theoretical value is maintained at approximately  $\alpha_T = 0.6$  regardless of the mesh density used. It can also be pointed out that in the vicinity of  $\alpha_T = 0.5$  the calculation error of the coefficient  $c_{11}$  is not very sensitive to the mesh density. In general, conditions in which  $\alpha = 0.5$  can be given in some of the elements, the method is less robust because it is affected by the singularity.

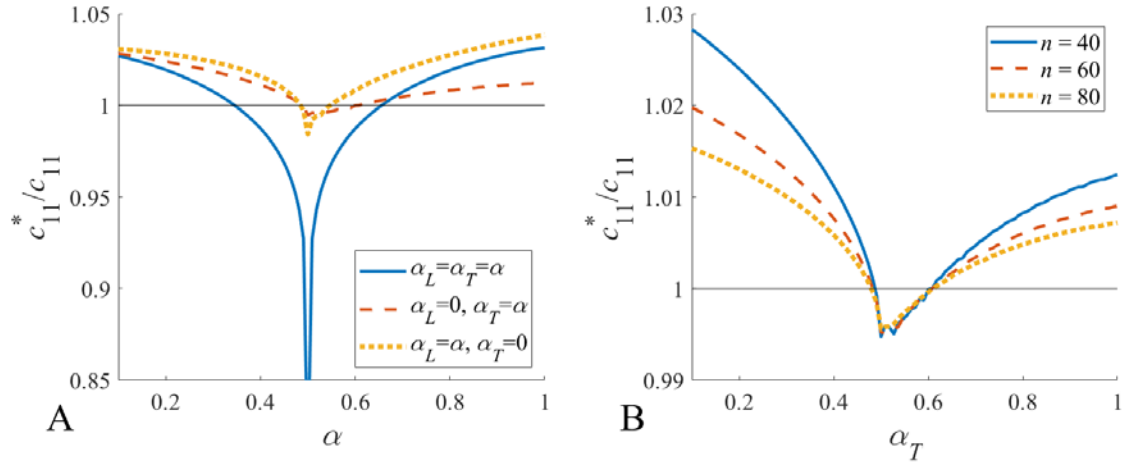


Fig.: 7.  $c_{11}^*/c_{11}$  ratio as a function of the collocation parameter  $\alpha$ . The derivative  $\partial u / \partial x$  is calculated through the closed form expression. A) Collocation method by means of three approaches:  $\alpha_L = \alpha_T = \alpha$ ;  $\alpha_L = 0$  and  $\alpha_T = \alpha$ ;  $\alpha_L = \alpha$  and  $\alpha_T = 0$ . The number of elements is  $n = 40$ . B) Collocation method by adopting  $\alpha_L = 0$  for three different number of elements:  $n = 40$ ,  $n = 60$  and  $n = 80$ .

Fig. 8 compares results that were carried out by approaching the derivatives by means of finite differences and by the closed form expression. They show that the calculation through finite differences gives better results than the exact calculation of the derivatives. This conclusion is more evident for the curves  $\alpha = 0.5$  for all the elements in which the effect of the derivative singularity is much more pronounced. Fig. 8.A analyses the case  $\alpha = 0.5$  versus the mesh density through both approaches. It must be pointed out that this study assumes that  $\alpha = 0.499$  when the closed form formula of the derivative is adopted.

In Fig. 8.B the case corresponding to  $\alpha_L = 0$  is studied. The accuracy of the results corresponding to the analytical formula of the derivatives is better than the results in Fig. 8.A. Although the best precision is also obtained for the calculation of derivatives by finite differences and  $\alpha_T = 0.63$ , for number of elements greater than 30 the accuracy obtained with the analytical formula and  $\alpha_T = 0.6$  is acceptable. The convergence speed is, however, smaller when the calculations are performed through the closed form expression and  $\alpha_T = 0.47$ .

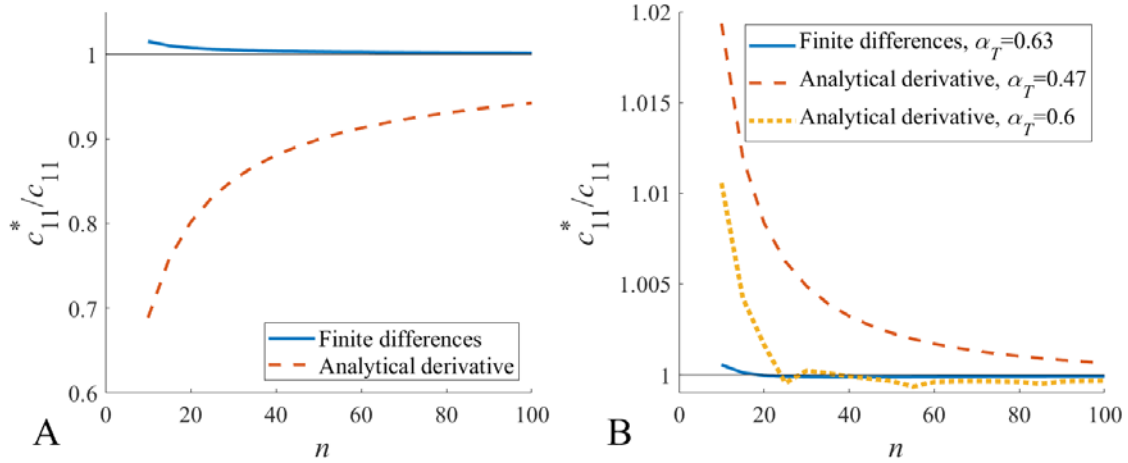


Fig. 8: Comparison between calculations performed through finite differences and the closed form expression of the derivative  $\partial u / \partial x$ . A)  $\alpha_L = \alpha_T = 0.5$ . B)  $\alpha_L = 0$  and  $\alpha_T = 0.63$  (if finite differences),  $\alpha_T = 0.47$  and  $\alpha_T = 0.6$  (if analytical derivative),

Another aspect of interest is to know the tangential traction distributions that are obtained through the different strategies analysed in previous sections. Fig. 9 presents calculations of the tangential traction that were obtained by means of the collocation method for  $\xi = 0.0001$ , using  $n = 40$  elements. Four strategies are assessed:

- Exact calculation of derivatives, collocation method,  $\alpha_L = \alpha_T = 1$ .
- Approximation by finite differences, collocation method,  $\alpha_L = \alpha_T = 0.5$ .
- Approximation by finite differences, collocation method,  $\alpha_L = 0$ ,  $\alpha_T = 0.63$ .
- Approximation by finite differences, collocation method,  $\alpha_L = \alpha_T = 1$ .

It can be seen that the traction distribution oscillates when  $\alpha_L = \alpha_T = 1$ , which does not appear in the other two strategies. It has been found that the oscillating response is calculated for values of parameter  $\alpha$  greater than 0.9. As a consequence, obtaining a smooth stress distribution requires using coefficients  $\alpha_L$  and  $\alpha_T$  smaller than 0.9. It should be pointed out that the strategy  $\alpha_L = \alpha_T = 1$  is equivalent to the one used by Knothe and Groß-Thebing in Ref. [15].

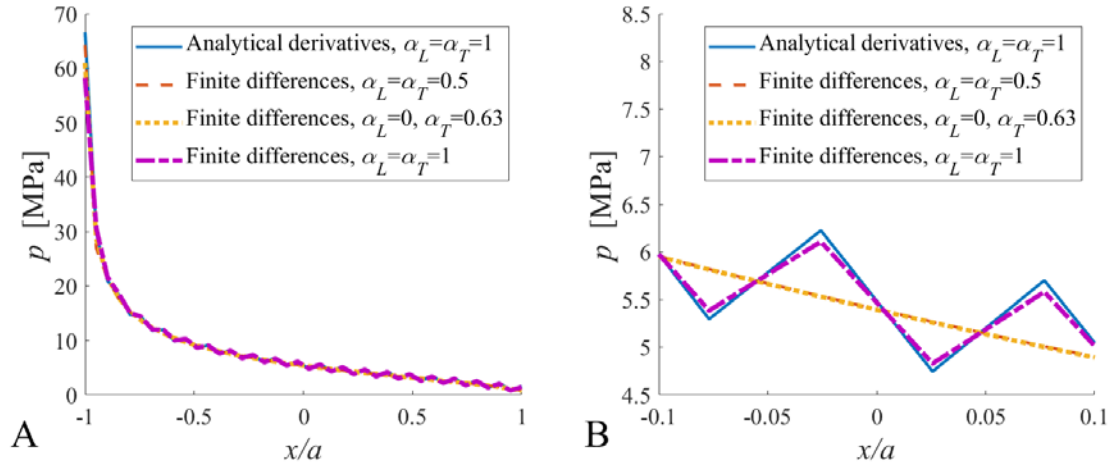


Fig. 9: Tangential traction distribution in the contact area. Calculation performed for  $\xi=0.0001$ , following three different strategies: (1) analytical derivatives when  $\alpha_L = \alpha_T = 1$ ; (2) finite differences when  $\alpha_L = \alpha_T = 0.5$ ; (3) finite differences when  $\alpha_L = 0$  and  $\alpha_T = 0.63$ .  
 A) Traction distribution in the whole area. B) Zoomed view.

Fig. 10 compares the tractions according to Carter [3] with the tractions obtained numerically when the derivatives are obtained by finite differences (the collocation method is used here with  $\alpha_L = 0$  and  $\alpha_T = 0.63$ ). It can be observed that, excepting the vicinity of the trailing edge of the contact area that is affected by the singularity, both distributions are practically indistinguishable, thus confirming the validity of the method.

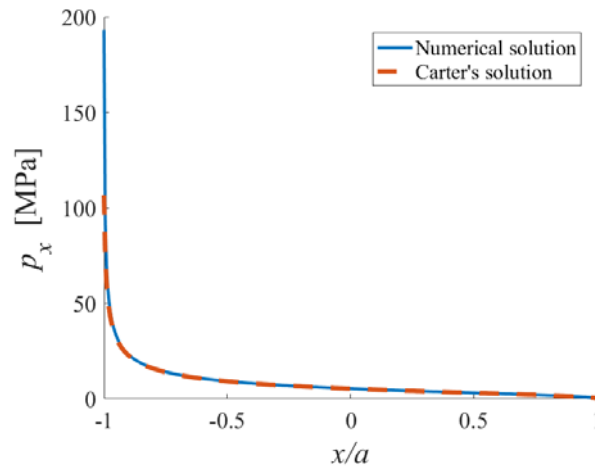


Fig. 10: Tangential traction distribution calculated by means of Carter's exact solution and the collocation method using collocation method is used here with  $\alpha_L = 0$  and  $\alpha_T = 0.63$ .

## 5.2. Galerkin method

The Galerkin method is an alternative approach for solving Eq. (15) numerically. It is formulated by means of Eq. (14), and the integrals in the latter are solved through quadrature with seven Gauss points. As in the case of the collocation method, it will be defined by the position of the Gauss points by means of parameter  $\alpha$ , which determines the shift of the Gauss points with respect to the centre of the element.

Fig. 11 presents results obtained through the Galerkin method using seven Gauss points. These results can be compared with those from Fig. 5 that were obtained by means of the collocation method. In Fig. 11, the ratio between the numerical and analytical creep coefficients  $c_{11}^*/c_{11}$  versus parameter  $\alpha$  is showed. The derivative of the displacements has been computed through finite differences. By comparing Fig. 11.A with Fig. 5.A, the curve  $\alpha_L = 0$  that obtains the best results, tends to give a minimum error for  $\alpha_T = \alpha = 1$ . Fig. 11.B shows that this trend is maintained when the number of elements  $n$  is increased.

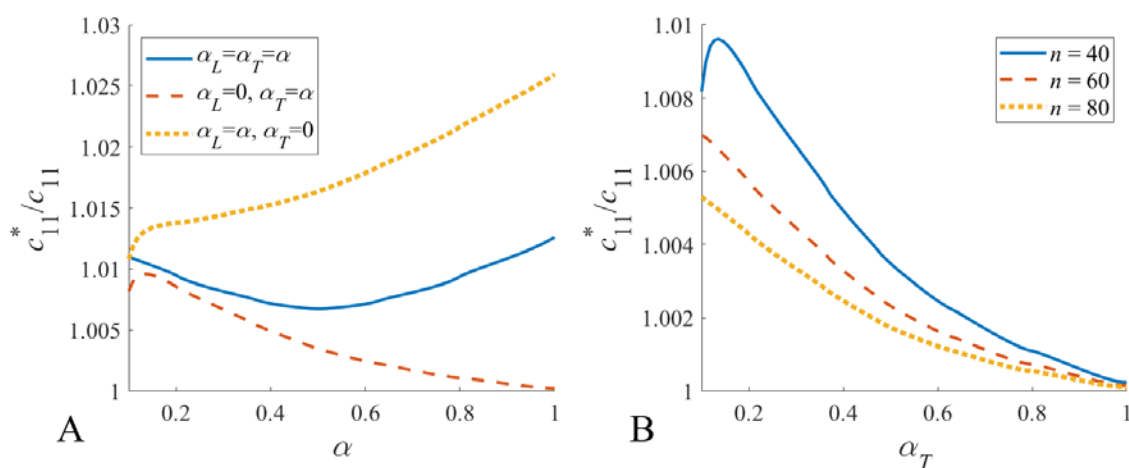


Fig. 11:  $c_{11}^*/c_{11}$  ratio as a function of parameter  $\alpha$ . The calculation has been carried out by means of Galerkin method, using 7 Gauss points. The derivative  $\partial u / \partial x$  is calculated through finite differences. A) Three different approaches:  $\alpha_L = \alpha_T = \alpha$ ;  $\alpha_L = 0$  and  $\alpha_T = \alpha$ ;  $\alpha_L = \alpha$  and  $\alpha_T = 0$ . The number of elements is  $n = 40$ . B) Collocation method by adopting  $\alpha_T = \alpha$  and  $\alpha_T = 0$ , for three different number of elements:  $n = 40$ ,  $n = 60$  and  $n = 80$ .

Fig. 12 corresponds to the calculation presented in Fig. 11.A, but in the present case the derivatives are calculated through the closed form expression. Fig. 12.A presents results where the integrals associated with the Galerkin formulation are computed by means of Gauss quadrature (seven Gauss points), whereas in Fig. 12.B these integrals are obtained analytically. The curves in Fig. 12.A are characterised by dips that are due to the coincidence of Gauss points and the element borders (where the analytical derivative is singular). Despite the

uncertainty associated with the presence of the singularity, a greater precision is observed in the curve  $\alpha_T = 0$ .

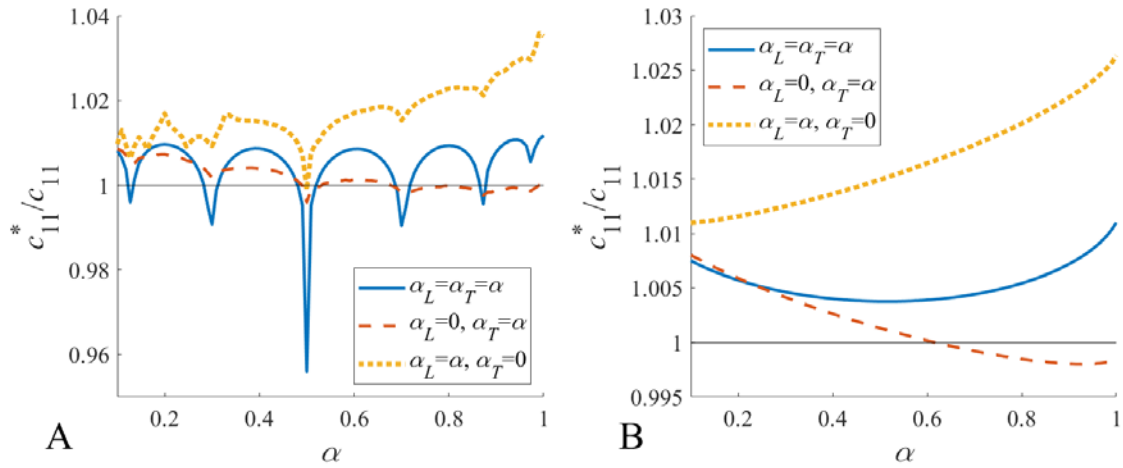


Fig. 12:  $c_{11}^*/c_{11}$  ratio as a function of parameter  $\alpha$ . The calculation has been carried out by means of Galerkin method. The derivative  $\partial u / \partial x$  is calculated through its closed form expression. Three different approaches have been studied:  $\alpha_L = \alpha_T = \alpha$ ;  $\alpha_L = 0$  and  $\alpha_T = \alpha$ ;  $\alpha_L = \alpha$  and  $\alpha_T = 0$ . The number of elements is  $n = 40$ . A) The numerical integration is done by means of quadrature with 7 Gauss points. B) Exact analytical integration.

It can be seen in Fig. 12.B that the analytical integration eliminates the effects of the derivative singularity. Again the curve  $\alpha_L = 0$  presents the best precision. Within this strategy, the most accurate results are obtained for  $\alpha_T = 0.63$ . An initially interesting result is that, in spite of the calculation methods being quite different, Fig. 12.B is coincident with Figure 5.A. According to these results, the collocation method using finite differences for calculating derivatives is equivalent to Galerkin with the analytical calculation of derivatives.

This fact is best seen in Fig. 13.A, which looks very similar to Fig. 5.B. Also in this case the three curves corresponding to the three mesh densities  $n = 40, 60$  and  $80$  reach 1 when  $\alpha_T = 0.63$ . Finally, Fig. 13.B reveals that Galerkin and the collocation method produces almost identical curves if  $\alpha_L = 0$  and  $\alpha_T = 0.63$  are adopted.

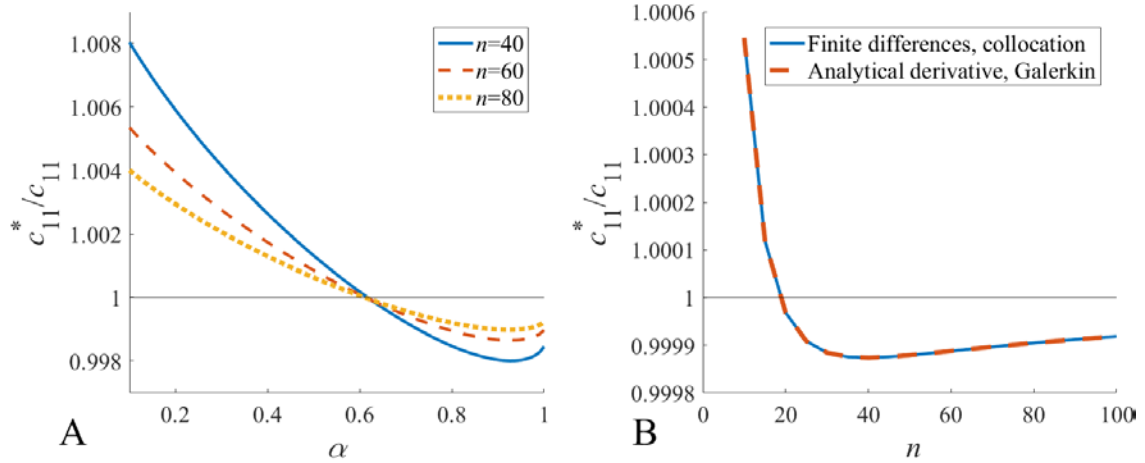


Figura 13. A)  $c_{11}^*/c_{11}$  ratio vs  $\alpha$  ( $\alpha_L = 0$  and  $\alpha_T = \alpha$ ). The calculation has been carried out by means of Galerkin method by using analytical integration. The derivative  $\partial u / \partial x$  is calculated through its closed form expression. Results from three mesh densities are presented. B)  $c_{11}^*/c_{11}$  ratio vs the number of elements in the mesh  $n$ . The calculations compare results from the collocation method (using finite differences) and the Galerkin method (using the analytical derivative).  $\alpha_L = 0$  and  $\alpha_T = 0.63$

### 5.3. Mesh topology

The present subsection assesses the mesh topologies that were shown in Fig. 4. These studies were carried out by adopting derivatives obtained by finite differences and the collocation method, and presents the ratio  $c_{11}^*/c_{11}$  for assessing the precision of the numerical method. The possibility of using a mesh with element size varying in geometric progression (shown in Fig. 4.B) has been analysed in Fig. 14. The element size is determined by means of the following criteria:

$$\Delta x_{i+1} = r \Delta x_i, \quad (32)$$

$r$  being the common ratio of the geometric progression. The results are plotted for three mesh densities as the function of the ratio between the mesh sizes of the leading and trailing elements. It can be seen in Fig. 14.A that the best results for a uniform mesh are obtained when  $\alpha_L = 0$ ,  $\alpha_T = 0.63$ . However for  $\alpha_L = \alpha_T = 0.5$  (Fig. 14.B) the optimal results corresponds to a ratio of the leading element size to the trailing element size, of 0.5. It should be noted in both cases that, due to the small influence on the results, the optimal value of the ratio is almost independent of the mesh density used.

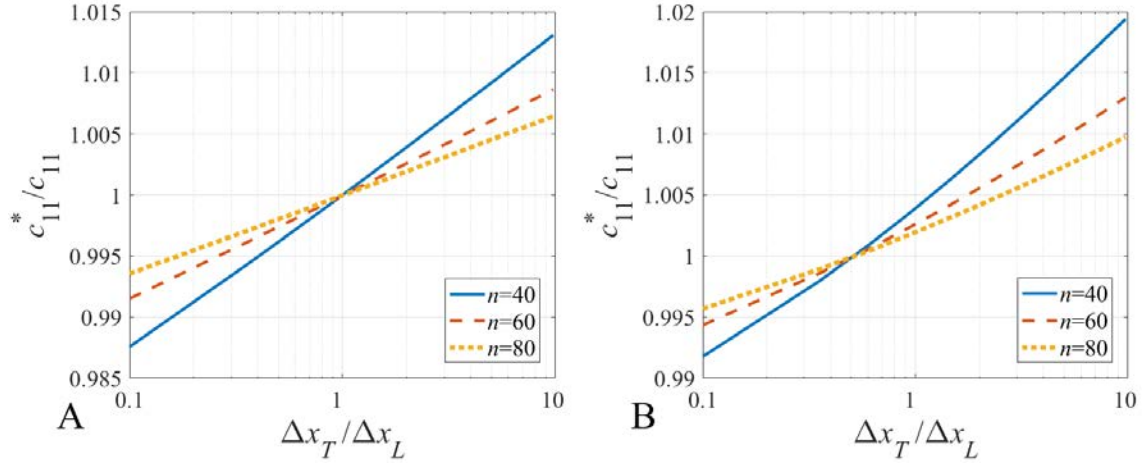


Fig. 14:  $c_{11}^*/c_{11}$  vs the ratio between the trailing and the leading element sizes  $\Delta x_T/\Delta x_L$  when the topology presented in Fig. 4.B (geometric refinement) is adopted. NB the abscissa axes are in logarithmic scale. A)  $\alpha_L = 0$  and  $\alpha_T = 0.63$ . B)  $\alpha_L = \alpha_T = 0.5$ .

Fig. 15 analyses the use of the topology adopted in Ref. [15]. In Knothe and Groß-Thebing's work, the size of the leading and trailing elements of the mesh is  $\varepsilon \Delta x$ , being  $\varepsilon$  a factor and  $\Delta x$  the size of the inner elements. The plots analyse the effect of factor  $\varepsilon$  on the ratio  $c_{11}^*/c_{11}$ : Fig. 15.A adopts  $\alpha_L = 0$  and  $\alpha_T = 0.63$ , whereas Fig. 15.B assumes  $\alpha_L = \alpha_T = 0.5$ . In Fig. 15.A, the optimal results are reached for  $\varepsilon = 1$  (uniform element size), whereas in Fig. 15.B the best results are found when  $\varepsilon = 0.4$ . The influence of  $\varepsilon$  is nevertheless small in both plots.

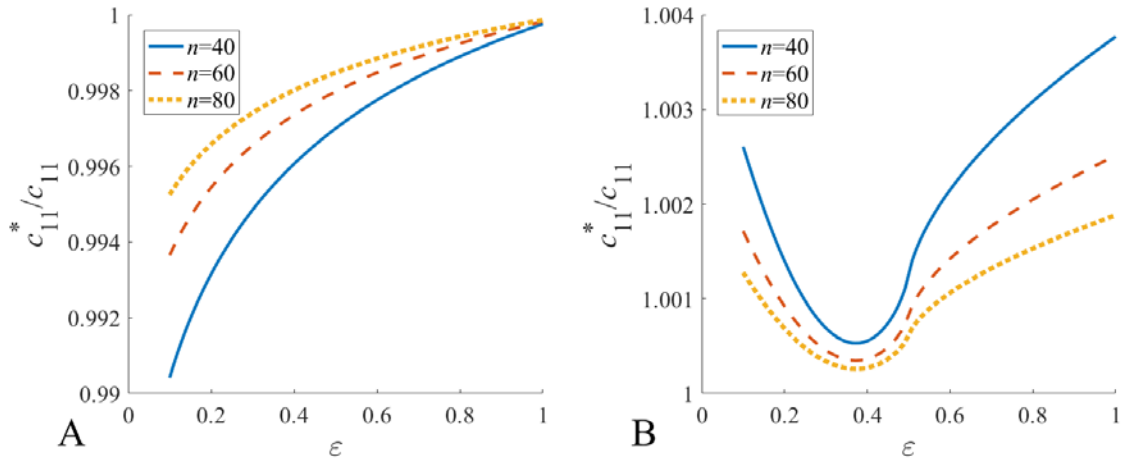


Fig. 15:  $c_{11}^*/c_{11}$  ratio vs coefficient  $\varepsilon$  when the mesh topology due to Knothe and Groß-Thebing is adopted. A)  $\alpha_L = 0$  and  $\alpha_T = 0.63$ . B)  $\alpha_L = \alpha_T = 0.5$ .

Fig. 16 presents  $c_{11}^*/c_{11}$  ratio versus factor  $\varepsilon$  when Knothe modified topology is adopted. The element-size is equal for all the elements, except the trailing one, which is  $\varepsilon \Delta x$ . The study has

been made for different mesh densities. Fig. 16.A adopts  $\alpha_L = 0$  and  $\alpha_T = 0.63$ , and the results present an optimum when  $\varepsilon$  is close to 1. Fig. 16.B, considers the case where  $\alpha_L = \alpha_T = 0.5$ , and it does not present any result without error. The best results are obtained for  $\varepsilon = 1$ , but its influence is small.

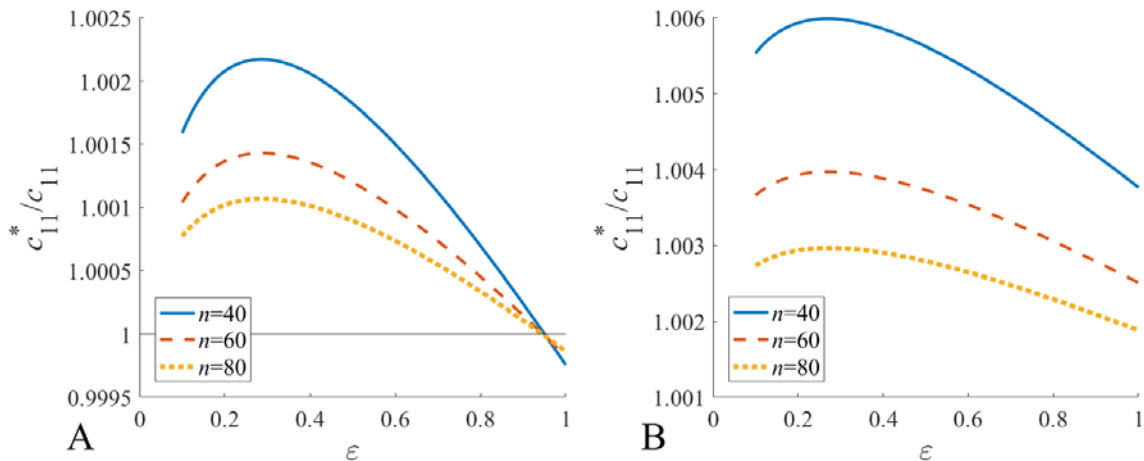


Fig. 16:  $c_{11}^*/c_{11}$  ratio vs coefficient  $\varepsilon$  when the Knothe modified topology is adopted. A)  $\alpha_L = 0.63$  and  $\alpha_T = 0$ . B)  $\alpha_L = \alpha_T = 0.5$ .

Fig. 17 shows the tangential traction distribution obtained through three different topologies (constant size elements, Knothe and Groß-Thebing, and modified Knothe topologies) and they are compared with the theoretical distribution deduced by Carter [3]. In most of the contact area (they are not plotted in the figure), the traction distributions of the three strategies are very coincident with Carter's distribution. However, on both edges, and especially on the trailing edge, very important differences can be seen between the different strategies. At the trailing edge (Fig. 17.A), Knothe and Groß-Thebing and modified Knothe topologies provide very similar traction distributions, and they overestimate the tractions calculated by Carter. The mesh with constant size elements is the one that most closely matches the Carter traction, although it should be noted that the point at which the traction is calculated in the constant size mesh is farther from the edge than in the modified Knothe and Knothe/Groß-Thebing topologies. At the leading edge (Fig. 17.B), the topologies according to modified Knothe and constant size mesh give very similar results; these are very close to the solution of Carter, although slightly higher. Knothe and Groß-Thebing's topology once again overestimates Carter's solution. Also in this case, the topologies that give less error in the estimation of the tractions provide the tractions in the points furthest from the edge.

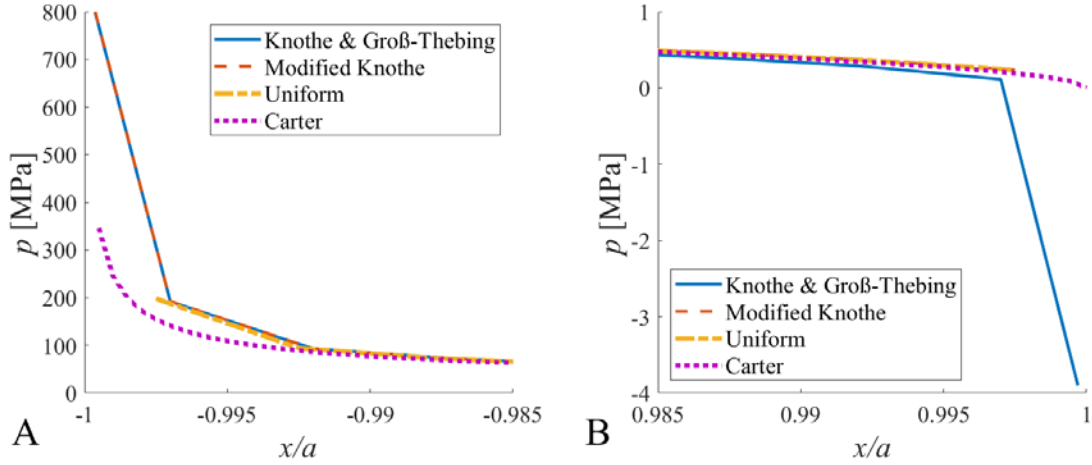


Fig. 17: Two zoomed views of the tangential traction distribution calculated through different mesh topologies. A) Trailing edge of the contact area. B) Leading edge of the contact area.

## 6. STUDY FOR THE 2D NON-STEADY STATE CASE

### 6.1. Stability

The numerical strategies used in the static calculation (and analysed in the previous section) are valid for a dynamic analysis as long as their stability is guaranteed. For the non-steady state case, from Eq. (12), the following generalised eigenvalue problem is found:

$$\mathbf{G}'\mathbf{p} = \nu \mathbf{G}\mathbf{p}. \quad (33)$$

For the system to be stable, all eigenvalues  $\nu_k$  must have negative real part. The present section will show that the stability of the proposed models is dependent on parameter that position the collocation and the Gauss points. To analyse the stability of each model, the proportion of unstable eigenvalues that are computed will be represented.

Fig. 18 plots the proportion of unstable eigenvalues as a function of  $\alpha$ . This study corresponds to the collocation method with  $\alpha = \alpha_L = \alpha_T$ . The calculations have been done for several mesh densities ( $n=20, 40$  and  $60$  elements). In Fig. 18.A the derivatives have been obtained analytically, whereas in Fig. 18.B the derivatives have been obtained by finite differences. It is observed that, in both cases, the system is stable when  $\alpha_L = \alpha = \alpha_T < 0.5$ .

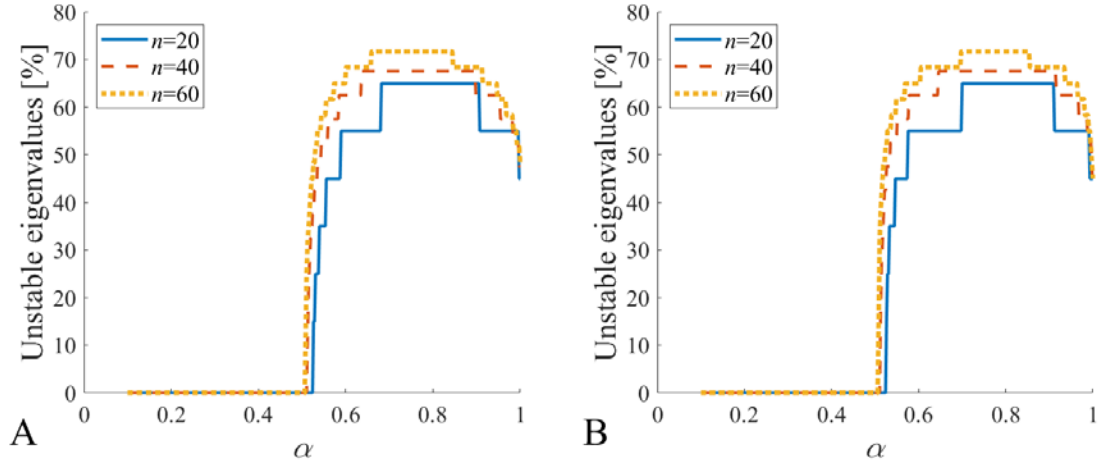


Fig. 18: Proportion of unstable eigenvalues in Eq. (33). Collocation method where  $\alpha = \alpha_L = \alpha_T$ . A) The derivative  $\partial u / \partial x$  is calculated through its closed form expression. B) The derivative  $\partial u / \partial x$  is calculated through finite differences.

Fig. 19 is analogous to the one presented in Fig. 18, but in the present case,  $\alpha_T$  are varied, keeping  $\alpha_L = 0$ . Both in the analytical and the numerical calculation of the derivatives, it is observed that  $\alpha_T < 0.7$  is required for the system to be stable. It is also observed that stability is more critical for higher mesh densities. In fact, if the number of cells is increased to very high values (this result is not included in this work), the stability requirement approaches  $\alpha_T < 0.5$ .

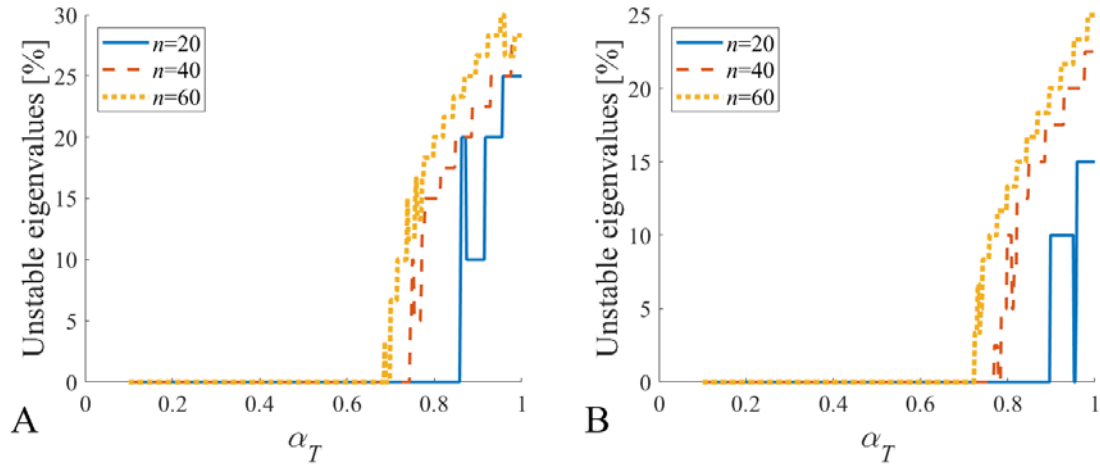


Fig. 19: Proportion of unstable eigenvalues in Eq. (33). Collocation method where  $\alpha_T$  varies and  $\alpha_L = 0$ . A) The derivative  $\partial u / \partial x$  is calculated through its closed form expression. B) The derivative  $\partial u / \partial x$  is calculated through finite differences.

Fig. 20 presents the proportion of unstable eigenvalues that have been calculated by means of the Galerkin method. The integrals are solved by numerical quadrature, using seven Gauss points. The figures represent the influence of  $\alpha$  on the proportion of unstable eigenvalues, when  $\alpha_L = 0$ . The calculations have been done for several mesh refinements ( $n = 20, 40$  and

60 elements). In Fig. 20.A the derivatives of the displacements have been calculated through the closed form expression, whereas in Fig. 20.B they have been calculated by means of finite differences. Through this scheme, the system is found to be stable when  $\alpha_T < 0.85$ , which indicates that this strategy is more stable than the collocation method. On the other hand, the calculation through finite differences is also more stable than the analytical calculation of the derivatives. It is also observed that stability is more critical for refined meshes (note that all eigenvalues are stable for  $n = 20$ ).

According to these results, strategies based on formulating the equations with shifts  $\alpha_L = \alpha = \alpha_T$  (the scheme that was adopted, for example, in Ref. [15]) give rise to unstable solutions and, although their results in steady state and in the frequency domain cases converge to the exact value, they could formally be questioned and must be avoided in the time domain. It should also be noted that, if dynamic stability has to be guaranteed,  $\alpha$  has to be smaller than 0.5.

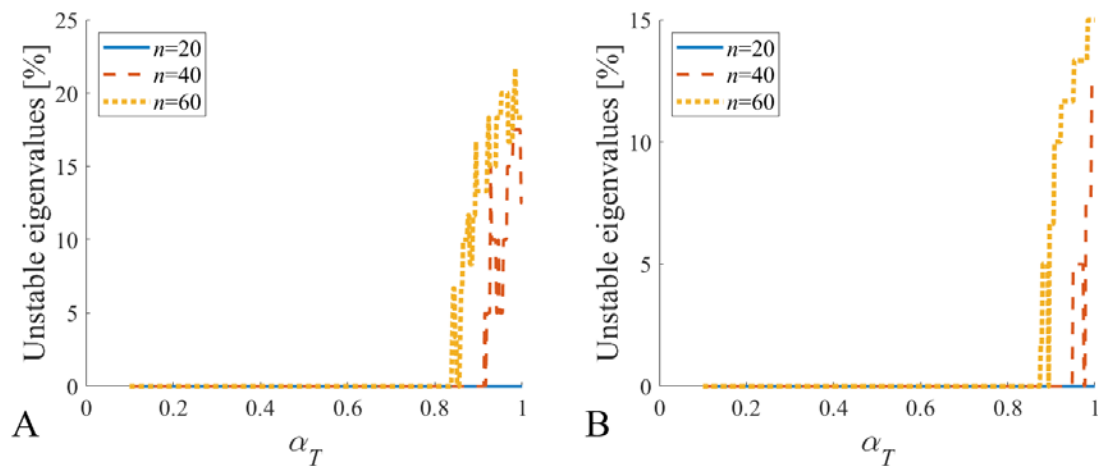


Fig. 20: Proportion of unstable eigenvalues in Eq. (33). Galerkin method where  $\alpha_T$  varies and  $\alpha_L = 0$ . A) The derivative  $\partial u / \partial x$  is calculated through its closed form expression. B) The derivative  $\partial u / \partial x$  is calculated through finite differences.

Fig. 21 studies the case where the matrices  $\mathbf{G}$  and  $\mathbf{G}'$  are obtained in different points. In these charts, matrix  $\mathbf{G}'$  is evaluated at points  $\alpha \Delta x$ , whereas matrix  $\mathbf{G}$  is calculated at points  $\lambda \alpha \Delta x$ , being  $\lambda$  one parameter between 0 and 1. The plots present the influence of  $\lambda$  on the proportion of unstable eigenvalues. The collocation method is adopted in these studies. In Figs. 21.A and 21.C the derivatives of the displacements have been calculated by means of the closed form expression, whereas the finite difference method is adopted in Figs. 21.B and 21.D; Figs. 21.A and 21.B adopt shifts  $\alpha_L = \alpha = \alpha_T = 1$ , while Figs. 21.C and 21.D make use of  $\alpha_L = 0$  and  $\alpha_T = 1$ . It can be seen that there is a tendency to stability when matrix  $\mathbf{G}$  is evaluated in collocation points that are behind the collocation points of matrix  $\mathbf{G}'$ . Even for the worst case

with  $\alpha_L = \alpha = \alpha_T = 1$  the eigenvalues are stable if  $\lambda < 0.5$ . The condition  $\lambda < 0.5$  guarantees stability for any  $\alpha_L$  and  $\alpha_T$  values.

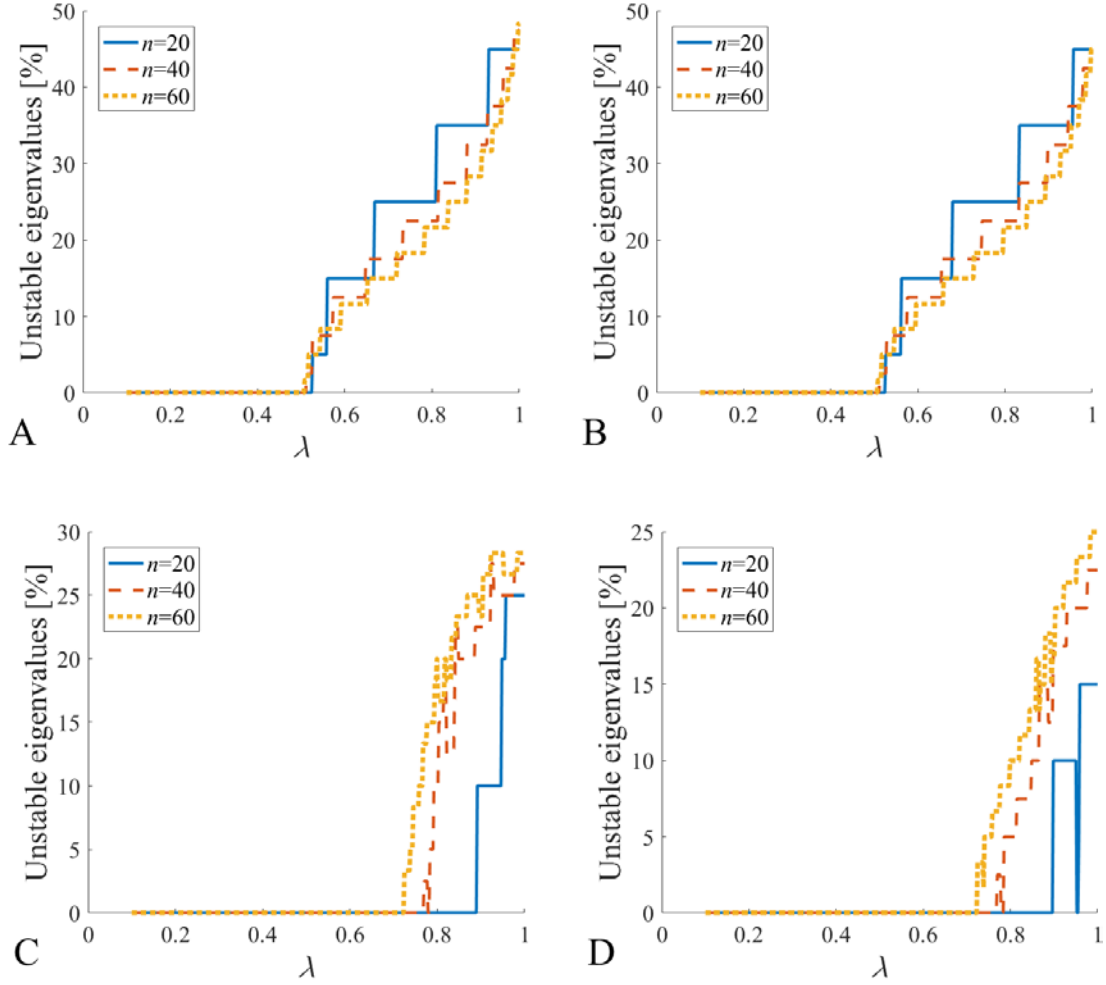


Fig. 21: Proportion of unstable eigenvalues in Eq. (33). Using the collocation method, matrix  $\mathbf{G}'$  is evaluated at  $x_e + \alpha \Delta x$  whereas  $\mathbf{G}$  is calculated at  $x_e + \lambda \alpha \Delta x$ . A) The derivative  $\partial u / \partial x$  is calculated through its closed form expression, and  $\alpha_L = \alpha_T = 1$ . B) The derivative  $\partial u / \partial x$  is calculated by means of finite differences, and  $\alpha_L = \alpha_T = 1$ . C) The derivative  $\partial u / \partial x$  is calculated through its closed form expression,  $\alpha_L = 0$  and  $\alpha_T = 1$ . D) The derivative  $\partial u / \partial x$  is calculated by means of finite differences,  $\alpha_L = 0$  and  $\alpha_T = 1$ .

## 6.2. Response in the frequency domain

Fig. 22.A plots in the complex plane, the creep coefficient  $c_{11}^*$  calculated through the collocation method for  $n = 20, 40$  and  $60$  elements. This calculation is compared with the reference solution obtained by means of the polynomial approach through the solution of Eqs. (25) to (27). The results show good agreement between the different methodologies. This good agreement can also be seen in Fig. 22.B, where the imaginary and real parts of the creep coefficient, versus the frequency, are represented. In this study the number of elements is  $n = 60$ , the order of the polynomial approach is 20 and the frequency is non-dimensional (it is

multiplied by  $a/V$ , being  $a$  one half of the contact area length and  $V$  the speed). In this range of frequencies, the polynomial method, though not presented in this figure, also produces accurate results, even if just a first order polynomial is adopted.

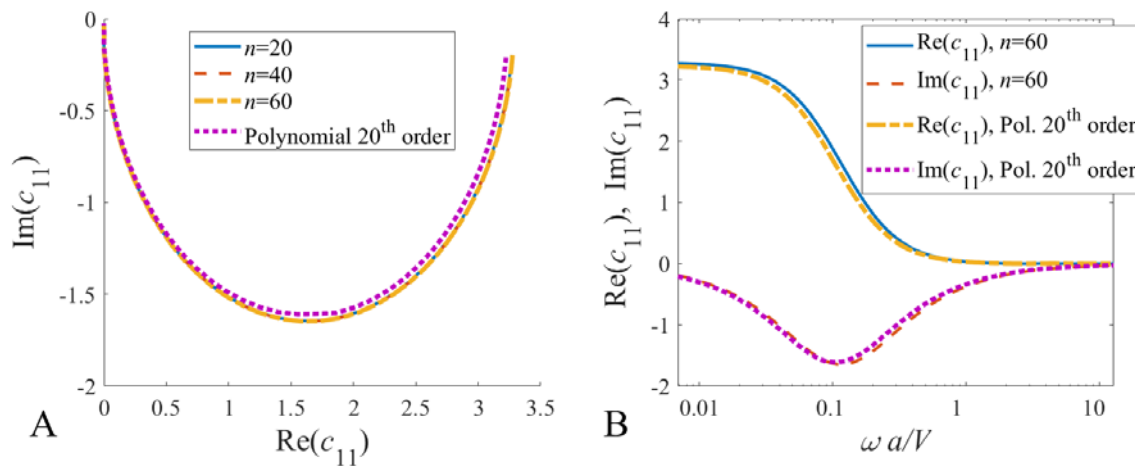


Fig. 22: Complex creep coefficient  $c_{11}^*$  associated with a harmonic creepage, calculated by means of the collocation method (the derivative  $\partial u / \partial x$  is calculated by means of finite differences,  $\alpha_L = 1$  and  $\alpha_T = 0$ ). The results are compared with the creep coefficient  $c_{11}$  through a polynomial approach. A) Creep coefficients in the Argand diagram, by using  $\omega$  as parameter. B) Real and imaginary part of creep coefficients vs the creepage frequency  $\omega$ .

## 7. CONCLUSIONS

This work presents a methodology for assessing the precision of the 2D tangential rolling contact calculation by means of the boundary element method (BEM). In order to solve the stationary problem, two different strategies have been analysed: the collocation method (based on CONTACT algorithm) and the Galerkin method. The calculation of the response to a harmonic creepage is carried out in this paper by means of the collocation method and a new development based on a polynomial approach that provides a solution to the unsteady contact problem. For calculating the derivative of the displacements  $\partial u / \partial x$ , two cases have been considered: the exact calculation of the derivative and its approximation by means of finite differences. This paper analyses different mesh topologies of the mesh, some already used by other authors and others that have been proposed within this work. In order to verify the degree of precision and effectiveness of the different strategies and topologies considered, they have been applied to two-dimensional problems by adopting steady and unsteady assumptions.

It has been verified that the approximation by means of differences is, in general, more robust than the exact calculation of the derivatives. To obtain accurate results in the calculation of derivatives, it is necessary to avoid their evaluation at the edges of the elements or in their vicinity.

The collocation method can be applied in different variants. The influence of shifting the collocation points has been analysed. It has been verified that the most efficient collocation strategy is achieved for the values  $\alpha_L = 0$  and  $\alpha_T = 0.63$ . Calculations based on the Galerkin method are much more computationally expensive and do not provide enough advantages to justify their use. In this sense, it has been verified that the use of the collocation method, combined with the estimation of derivatives by finite differences, is equivalent to the Galerkin method with the exact calculation of integrals and derivatives.

Different topologies have been tested, verifying that the most efficient collocation strategy ( $\alpha_L = 0$  and  $\alpha_T = 0.63$ ) with identical element size meshes is the more efficient. However, other topologies with different values of  $\alpha_L$  and  $\alpha_T$  can provide even better results. Regarding the traction distribution within the contact area, values of  $\alpha_L$  and  $\alpha_T$  greater than 0.9 give rise to an oscillating distribution of  $p$  tractions; it is therefore advisable to adopt lower values.

The dynamic stability of the contact equations has been analysed in this paper, detecting that large values of  $\alpha_L$  and  $\alpha_T$  produce unstable responses. If  $\alpha_L = \alpha_T$ , it is necessary to ensure that these values are smaller than 0.5. The use of the Galerkin method also improves the stability with respect to the collocation method, requiring higher values of  $\alpha$  parameter and/or higher mesh densities for having unstable eigenvalues. One way to improve the stability is by adopting different collocation points in the calculation of matrices  $\mathbf{G}$  and  $\mathbf{G}'$ .

The dynamic response analysis through the collocation method, compared with the results obtained by a polynomial approximation similar to that used by Kalker for the steady case [5], results in correlation levels similar to those obtained in the static case.

## ACKNOWLEDGEMENTS

The authors gratefully acknowledge the financial support of the Spanish Ministry of Economy, Industry and Competitiveness and the European Regional Development Fund (project TRA2017-84701-R), as well as the European Commission through the projects "RUN2Rail - Innovative RUNning gear soluTiOns for new dependable, sustainable, intelligent and comfortable RAIL vehicles" (Horizon 2020 Shift2Rail JU call 2017, grant number 777564) and 'PIVOT - Performance Improvement for Vehicles On Track' (Horizon 2020 Shift2Rail JU call 2017, grant number 777629).

## REFERENCES

- [1] D. Thompson, Railway noise and vibration: Mechanisms, modelling and means of control, Elsevier, Oxford, UK, 2008.
- [2] L. Rodriguez-Tembleque, R. Abascal, M.H. Aliabadi, Anisotropic wear framework for 3D contact and rolling problems, *Comput Method Appl M*, 241 (2012) 1-19.

- [3] F.W. Carter, On the action of a locomotive driving wheel, Proceedings of the Royal Society of London. Series A, 112 (1926) 151-157.
- [4] J.J. Kalker, The transmission of force and couple between two elastically similar spheres, Proceedings Koninklijke Nederlandse Academie v. Wetenschappen, 67 (1964) 135-177.
- [5] J.J. Kalker, On the rolling contact of two elastic bodies in the presence of dry friction, PhD Thesis, Delft University of Technology, 1973.
- [6] J.J. Kalker, Two algorithms for the contact problem in elastostatics, in: J. Kalousek, R.V. Dukkipati, G.M.L. Gladwell (Eds.) Contact Mechanics and Wear of Wheel-Rail Systems 1982, University of Waterloo Press, Vancouver, 1983, pp. 101-120.
- [7] J.J. Kalker, Variational principles of contact elastostatics, IMA Journal of Applied Mathematics, 20 (1977) 199-219.
- [8] J.J. Kalker, Three-Dimensional Elastic Bodies in Rolling Contact, Springer Netherlands, Dordrecht, 1990.
- [9] J. Giner, L. Baeza, P. Vila, A. Alonso, Study of the Falling Friction Effect on Rolling Contact Parameters, Tribol Lett, 65 (2017).
- [10] J.J. Kalker, A Fast Algorithm for the Simplified Theory of Rolling Contact, Vehicle System Dynamics, 11 (1982) 1-13.
- [11] J.G. Giménez, A. Alonso, E. Gómez, Introduction of a friction coefficient dependent on the slip in the FastSim algorithm, Vehicle System Dynamics, 43 (2005) 233-244.
- [12] A. Guiral, A. Alonso, L. Baeza, J.G. Gimenez, Non-steady state modelling of wheel-rail contact problem, Vehicle System Dynamics, 51 (2013) 91-108.
- [13] L. Baeza, P. Vila, A. Roda, J. Fayos, Prediction of corrugation in rails using a non-stationary wheel-rail contact model, Wear, 265 (2008) 1156-1162.
- [14] G.D. Hu, P. Wriggers, On the adaptive finite element method of steady-state rolling contact for hyperelasticity in finite deformations, Comput Method Appl M, 191 (2002) 1333-1348.
- [15] K. Knothe, A. Gross-Thebing, Derivation of Frequency Dependent Creep Coefficients Based on an Elastic Half-Space Model, Vehicle System Dynamics, 15 (1986) 133-153.
- [16] L.A. Galin, Contact Problems in the Theory of Elasticity, Department of Mathematics, School of Physical Sciences and Applied Mathematics, North Carolina State College, 1961.